

Double resonance Raman spectroscopy of single-wall carbon nanotubes

To cite this article: R Saito *et al* 2003 *New J. Phys.* **5** 157

View the [article online](#) for updates and enhancements.

Related content

- [First and Second-Order Resonance Raman Process in Graphite and Single Wall Carbon Nanotubes](#)
Riichiro Saito, Ado Jorio, Antonio G. Souza Filho et al.
- [Raman spectroscopy for probing chemically/physically induced phenomena in carbon nanotubes](#)
A G Souza Filho, A Jorio, Ge G Samsonidze et al.
- [Characterizing carbon nanotube samples with resonance Raman scattering](#)
A Jorio, M A Pimenta, A G Souza Filho et al.

Recent citations

- [Deep-ultraviolet Raman scattering spectroscopy of monolayer WS₂](#)
Hsiang-Lin Liu *et al*
- [Evolution of morphology and defect states in mechanically processed ZnO+xMWCNTs nanosystems](#)
Mykola Kakazey *et al*
- [Structural, optical and gas sensing properties of vertically well-aligned ZnO nanowires grown on graphene/Si substrate by thermal evaporation method](#)
Tran Van Khai *et al*



IOP | ebooks™

Bringing you innovative digital publishing with leading voices to create your essential collection of books in STEM research.

Start exploring the collection - download the first chapter of every title for free.

New Journal of Physics

An Institute of Physics and Deutsche Physikalische Gesellschaft Journal

Double resonance Raman spectroscopy of single-wall carbon nanotubes

R Saito¹, A Grüneis¹, Ge G Samsonidze², V W Brar²,
G Dresselhaus², M S Dresselhaus², A Jorio³, L G Cançado³,
C Fantini³, M A Pimenta³ and A G Souza Filho⁴

¹ Department of Physics, Tohoku University and CREST JST, Aoba Sendai 980-8578, Japan

² Massachusetts Institute of Technology, Cambridge, MA 02139-4307, USA

³ Departamento de Física, Universidade Federal de Minas Gerais, Caixa Postal 702, Belo Horizonte-MG 30123-970, Brazil

⁴ Departamento de Física, Universidade Federal do Ceará, Fortaleza-CE 60455-760, Brazil

New Journal of Physics 5 (2003) 157.1–157.15 (<http://www.njp.org/>)

Received 23 July 2003

Published 3 December 2003

Abstract. A review of double resonance Raman spectroscopy is presented. Non-zone centre phonon modes in solids can be observed in the double resonance Raman spectra, in which weak Raman signals appear in a wide frequency region and their combination or overtone modes can be assigned. By changing the excitation laser energy, we can derive the phonon dispersion relations of a single nanotube.

Contents

1 Introduction	2
2 General idea of resonance Raman spectroscopy	2
3 D and G' bands of graphite	4
4 D band of nanotube	10
5 Other intermediate phonon modes	12
6 Summary	13
Acknowledgments	14
References	14

1. Introduction

Carbon nanotubes have become a standard material in nanotechnology and a wide variety of applications using nanotubes have been proposed and investigated intensively (see this special issue, and also [1]). One of the most important subjects for nanotube technology is to evaluate nanotubes in a simple and quick way. In fact, we need to evaluate samples regarding the following points: (a) the purity of nanotubes, (b) diameter and chirality, (c) whether metallic or semiconducting, (d) whether a perfect or defective crystal. Raman spectroscopy is a non-destructive, non-dissipative measurement which is made at room temperature and at ambient pressure. In particular, resonance Raman spectroscopy can select a few nanotubes in the nanotube sample which are resonant with the excitation laser energy. Thus we can observe the properties of a nanotube by resonance Raman spectroscopy even for a bundle of nanotubes. A detailed description of the use of this technique for evaluating the above points is given in the paper by Jorio *et al* [2]. In the present paper we focus our attention on the so-called double resonance Raman spectroscopy.

In the following section, we give the general ideas behind resonance Raman spectroscopy and of the double resonance Raman process. Then we review the topic of double resonance Raman spectroscopy of graphite and carbon nanotubes.

2. General idea of resonance Raman spectroscopy

First we give the basic idea of resonance Raman spectroscopy [3, 4] for general readers. For a photo-excited electron, it will experience some processes before recombining with a hole in the valence energy band. One of these processes is a scattering process by a quantized lattice vibration known as a phonon with the phonon wave vector q . The electronic wave vector k is scattered to $k - q$ (phonon emission) or $k + q$ (absorption), respectively, and the electron energy is shifted downward or upward by $\hbar\omega_q$, which is given by observation of the scattered light and is known as the Stokes or anti-Stokes Raman shift. If a one-phonon scattering event occurs, it is called a first-order Raman process. If either the initial k or the scattered $k \pm q$ electronic states is a real electronic state, the scattering amplitude is enhanced, and this is known as the initial or scattered resonance Raman process, respectively (see figure 1(a1, a2)). This resonance enhancement is understood by quantum mechanical perturbation theory, where the energy difference denominator for the scattering amplitude becomes zero.

One important aspect of the Raman process in a crystal is that the photo-excited electron has to go back to its original k state to recombine with the hole at the k state. Because of this restriction, only a $q \sim 0$ phonon wave vector is selected in the first-order Raman process. Thus, in standard solid state textbooks, we see the statement that only the phonon energy at the centre (Γ point) of Brillouin zone, which is called the zone-centre phonon mode, is observed by Raman spectroscopy for solids.

We also expect second-order Raman processes to occur (figure 1(c1, c2)), by emitting (1) two phonons with the same frequency or (2) two phonons with different frequencies, which are called overtone or combination Raman modes, respectively. Another second-order process is given by one-phonon scattering and one elastic scattering process (figure 1(b1–b4)). Elastic scattering occurs in the presence of a defect in the crystal. In the latter case, the one-phonon energy is observed in the second-order process. Hereafter, we define the latter case also as a kind of second-order Raman process and we specify it as a one-phonon, second-order process.

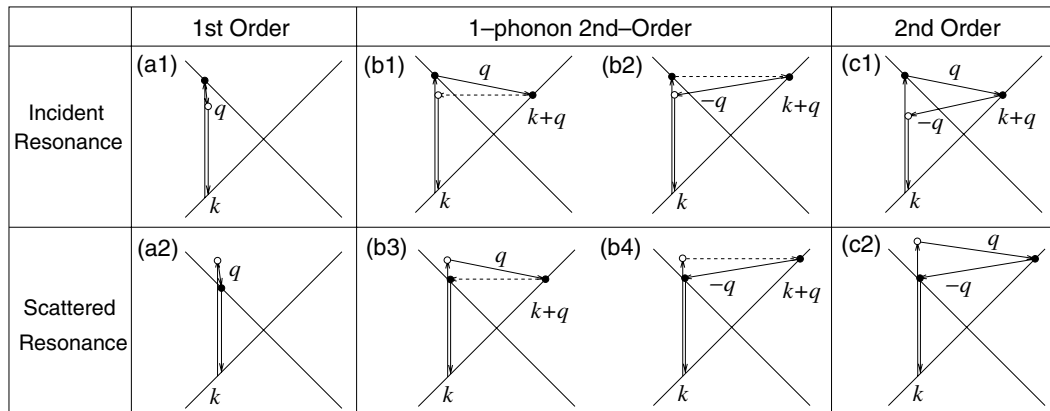


Figure 1. (a1, a2) First-order, (b1–b4) one-phonon second-order and (c1, c2) two-phonon second-order, resonance Raman spectral processes. Top panels: incident photon resonance; bottom panels: scattered resonance conditions. For one-phonon, second-order transitions, one of the two scattering events is elastic scattering (dashed line). Resonance points are shown as solid circles. See the text for details.

In a second-order process, since an electron is represented by wave vectors q and $-q$, respectively, by scattering from and then by back-scattering to the original k state, non-zone-centre phonon modes ($q \neq 0$) can be observed in the second-order Raman spectra. That is, (1) the electron is excited at k , (2) scattered to $k + q$, (3) scattered back to k and (4) recombined with a hole at k (see figure 1(b1–b4) and (c1, c2)). However, the probability for an electron to be scattered by a phonon (the Raman cross section) is generally small, and thus the probability for the event occurring twice in a second-order process is much smaller. Moreover, since q values can be arbitrary in the second-order process, the Raman spectra for the second-order Raman process generally becomes broad in the case of a crystal. Thus higher-order Raman processes in solids have not been considered much except for double resonance Raman spectroscopy [3].

In a double resonance process, the resonance enhancement results in Raman intensities that are almost of the same order as in the first-order resonance Raman spectra [4], and the corresponding q is selected by the resonance condition. For a one-phonon second-order process, we can expect four different double resonance Raman processes, as shown in figure 1(b1–b4). When we measure the electron energy from that of the valence band at k , the four resonant conditions of figure 1(b1–b4) can be expressed, respectively, by

- (b1) $E^i(k) = E_{\text{laser}}, E(k + q) = E^i(k) - \hbar\omega_{\text{ph}}(q), E^f(k) = E(k + q),$
- (b2) $E^i(k) = E_{\text{laser}}, E(k + q) = E^i(k), E^f(k) = E(k + q) - \hbar\omega_{\text{ph}}(-q),$ and
- (b3) $E^i(k) = E_{\text{laser}}, E(k + q) = E^i(k) - \hbar\omega_{\text{ph}}(q), E^f(k) = E(k + q),$
- (b4) $E^i(k) = E_{\text{laser}}, E(k + q) = E^i(k), E^f(k) = E(k + q) - \hbar\omega_{\text{ph}}(-q).$

In the above set of equations, the bold face letters imply the existence of a real electronic state. In the case of graphite, these four processes will give two different phonon frequencies in the D band which will be shown in the next section. In the anti-Stokes process, we simply consider the time-reversal counterpart of the corresponding Stokes process, and thus we have

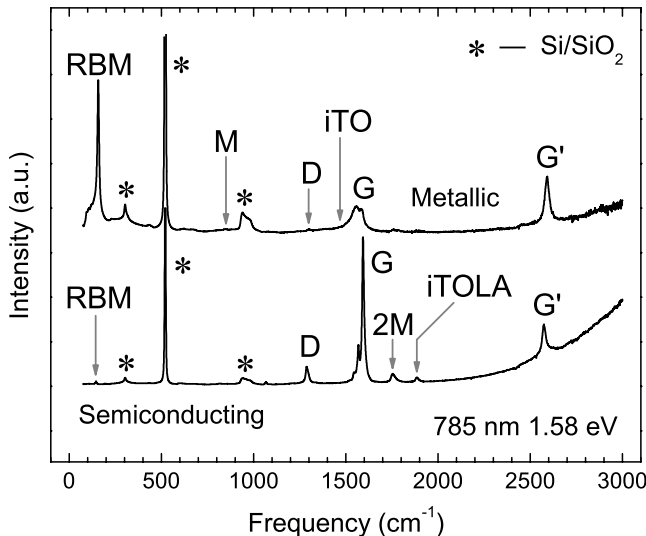


Figure 2. D and G' bands for a metallic (top) and a semiconducting (bottom) SWNT at the single nanotube level using 785 nm (1.58 eV) laser excitation. First-order Raman spectra, of the radial breathing mode (RBM), and G-band features, in addition to weak double resonance features associated with the M-band and the iTOLA second-order modes [8] (see the following sections) are shown. * denotes non-resonant Si Raman spectra from the Si/SiO₂ substrate, which are used for calibration purposes [9].

four corresponding anti-Stokes processes. For a two-phonon Stokes process, such as the G' band, the elastic scattering process denoted by a dashed line in figure 1(b1–b4) is changed to an inelastic phonon emission process. Then, only the cases (c1) and (c2) of figure 1 are possible for two-phonon double resonance processes.

For the one-dimensional (1D) carbon nanotube, the k and q vectors are quantized along the circumferential direction so that the values of k and q are selected with more stringent conditions [5, 6]. This is the reason why we observe sharp double resonance Raman peaks in carbon nanotubes. In fact, the line width of the D band of an SWNT is much smaller (as low as 7 cm^{-1}) than that for graphite ($\sim 50\text{ cm}^{-1}$). Because of the van Hove singularity in the joint density of states (JDOS), we expect an additional, significant enhancement of the Raman intensity [7].

In the following we will consider each of the important cases of the double resonance Raman spectra of graphite and nanotubes.

3. D and G' bands of graphite

D- and G'-band features are observed in the Raman spectra of graphite material at around 1355 and 2700 cm^{-1} , respectively for a laser excitation energy $E_{\text{laser}} = 2.41\text{ eV}$ [7], [10]–[13]. Neither of them are group-theory predicted, as first-order Raman spectra [14, 15]. In figure 2, we show typical D and G' band Raman spectra of single wall carbon nanotubes (SWNTs) in metallic (top) and semiconducting (bottom) nanotubes. In figure 2, we can also see first-order Raman spectra, such as the radial breathing modes (RBM) and the G band at

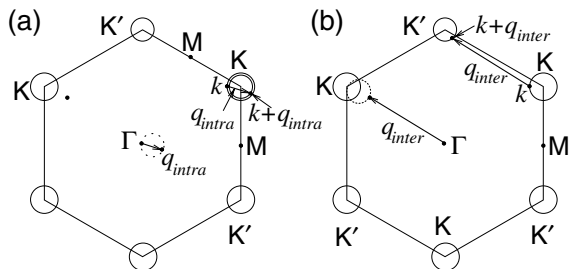


Figure 3. Energy contours of $E = E^i(k)$, $E(k + q)$ and $E^f(k)$ are shown as solid circles around the hexagonal corners of the K or K' points in the 2D Brillouin zone of graphite. Solid vectors with q_{intra} and q_{inter} denote, respectively, (a) an intra-valley and (b) an inter-valley scattering from a given k vector, shown near the upper-right K point. When we measure these q vectors from the Γ point, denoted by dotted vectors, q_{intra} and q_{inter} lie, respectively, on a dotted circle around the Γ and K points for the given k vector [16].

around 150 and 1590 cm^{-1} , respectively, and the other weak Raman features which will be discussed in the last section. Since the frequency of the G' band is close to twice that of the D-band frequency, the G' band is an overtone mode of the D band. Although the D and G' bands have been observed for more than 20 years, no clear explanation for the physical origin was available until the recent work on double resonance theory [7, 13, 16].

The D and G' bands show several unique Raman features.

Feature 1. The D- and G'-band frequency increases with increasing laser excitation energy, E_{laser} , in the visible light energy range. The values of the slope of the frequency with increasing laser energy are $\partial\omega_D/\partial E_{\text{laser}} = 53\text{ cm}^{-1}\text{ eV}^{-1}$ and $\partial\omega_{G'}/\partial E_{\text{laser}} = 106\text{ cm}^{-1}\text{ eV}^{-1}$ for the D and G' bands, respectively [17]–[20].

Feature 2. The D-band Raman intensity is large comparable to that of the first-order Raman G band when the sample has a large number of defects, while the G' band always shows a large intensity comparable to the G band without defects. Thus the D-band Raman intensity relative to the G-band intensity provides a good index for showing the presence of defects in graphite materials [18, 19], [21]–[23].

Feature 3. The G'-band frequency is not exactly twice that of the D-band frequency. The Stokes and anti-Stokes Raman frequencies of the D (or G') band are not exactly the same [25].

The D- and G'-band features are explained, respectively, by one-phonon and two-phonon, second-order Raman scattering processes using double resonance theory [7, 13, 16].

In 2D graphite, the optical transition occurs around the K point (the corners of the hexagonal Brillouin zone (BZ) (see figure 3)) where the bonding and anti-bonding π bands touch each other [14]. The bonding and anti-bonding electronic π bands show a linear k dispersion relation around the K point within the first approximation, as is already shown in figure 1,

$$E(k) = \pm \frac{\sqrt{3}}{2} \gamma_0 k a, \quad (1)$$

where the electronic k vectors are measured from the K point, $a = \sqrt{3}a_{\text{C-C}} = 2.46\text{ \AA}$ and $\gamma_0 = 2.89\text{ eV}$ [14]. Thus when E_{laser} increases, the electron k vectors and the corresponding phonon q vectors both increase.

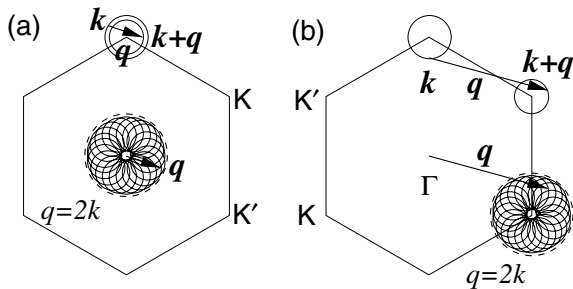


Figure 4. Possible q state for (a) intra-valley and (b) inter-valley scattering from k to $k + q$ states around K and K' points. When we start at q vector from the Γ point, the final q states are circles rotating around the (a) Γ point and (b) K (or K') point. The density of states for q is singular at $q \sim 2k$ (dashed circles) and $q \sim 0$ measured from the (a) Γ and (b) K points [25].

In figure 3, we show the energy contours of $E = E^i(k)$, $E(k + q)$ and $E^f(k)$ as solid circles around the K or K' points for the initial and intermediate states. The circle for $E^f(k)$ (or $E(k + q)$ in the cases of (b1) and (b3) in figure 1) is slightly smaller by the phonon energy than that for $E^i(k)$. Here there are two possibilities for selecting the phonon q vectors which satisfy the double resonance condition, as shown in figure 3, since there are two inequivalent corners (K and K' points) in the hexagonal BZ. One possibility for q is phonon scattering within the same K (or K') point denoted by q_{intra} (figure 3(a)) and the other is phonon scattering from the K to K' point (or from the K' to K point) denoted by q_{inter} (figure 3(b)), which we call intra-valley and inter-valley scattering, respectively. Since equi-energy lines of electronic energy around the K or K' points are circles, the possible q vectors can lie on circles rotated around the Γ or K points for intra-valley or inter-valley scattering processes. In figure 4 we show this situation for the cases of (a) intra-valley and (b) inter-valley scattering. It is noted that the difference in diameter for the two circles for k and $k + q$ in figure 4 is for clarity taken to be much larger than for the real case. Thus, possible regions of q are within a large circle whose diameter is close to $2k$ measured from the centre of the large circle. However, when we consider the phonon density of states which satisfies the double resonance condition, there are singular points at $q \sim 0$ and $q \sim 2k$ in the phonon density of states [25]. Thus we can observe $q \sim 0$ and $q \sim 2k$ phonon modes as double resonance modes. For $q \sim 2k$ phonon modes, q is selected as $2k$ which is a function of E_{laser} . When we see the phonon dispersion relation of graphite (see figure 5 (b)), there is only the 1350 cm^{-1} phonon energy around the K point, and we can assign D- and G'-band phonons as the intervalley scattering phonons around the K point. In the case of the G' band, since the Raman shift becomes approximately twice that of the D band, the slope of the dispersive $\partial\omega_{\text{G}}/\partial E_{\text{laser}}$ becomes twice that of $\partial\omega_{\text{D}}/\partial E_{\text{laser}}$. This is the reason for Feature 1.

As discussed in the previous section, in the case of the D band, one of the two scattering processes is not phonon-related scattering, but is rather elastic scattering by a defect. On the other hand, since the G' band corresponds to two-phonon processes, we do not need defects for the G'-band scattering processes, thus providing an explanation for the difference between the D- and G'-band properties (Feature 2).

Figure 5(a) plots the E_{laser} dependence of the frequency of the peaks in the density of (k, q) pairs [16]. The upper axis of the figure correlates the E_{laser} (lower axis) values with the phonon

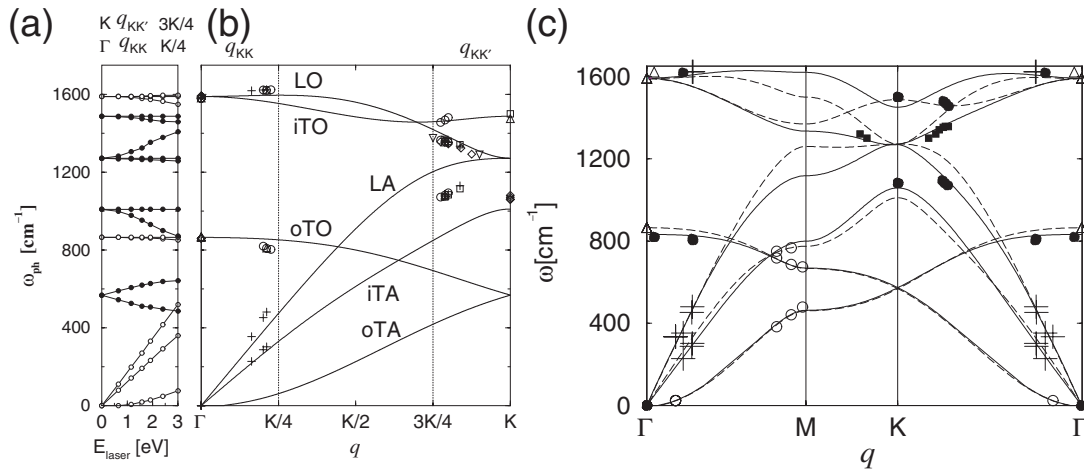


Figure 5. (a) Calculated Raman frequencies for the double resonance condition as a function of E_{laser} (bottom axis) and q vector along Γ –K (top axis). Solid and open circles correspond to phonon modes around the K and Γ points, respectively. (b) The six graphite phonon dispersion curves (lines) and experimental Raman observations (symbols) placed according to the double resonance theory. \circ , PG [26]; \square , C-HOPG [27]; \triangle , HOPG [26, 28]; \diamond , SWNT [17, 29, 30]; $+$, GW [31]; ∇ , MG [18]. See text for the definition of sp^2 carbons [16]. (c) Phonon dispersion relations of 2D graphite fitted to double resonance Raman spectroscopy [32].

wave vector q related to each peak. It is noted that the linear relationship between E_{laser} and q is valid for $E_{laser} \leq 3.0$ eV. Solid and open circles correspond to the phonon modes around the K ($q_{KK'}$) and Γ (q_{KK}) points, respectively. Along the Γ –K direction, q_{KK} changes from Γ to $\sim \frac{1}{4}K$ as E_{laser} increases from 0 to 3.0 eV, while $q_{KK'}$ changes from K to $\sim \frac{3}{4}K$, so that $\frac{1}{2}$ of the BZ along Γ –K is probed by this range of E_{laser} . Figure 5(b) shows the graphite phonon dispersion relations in the Γ –K direction [14, 33]. Vertical dotted lines show the limits for the q_{KK} and $q_{KK'}$ wave vectors imposed by $E_{laser} \leq 3.0$ eV.

By using the $E_{laser} \leftrightarrow q$ relations given in figure 5(a), we can take experimental values from several published papers giving Raman frequencies observed using different laser lines for various sp^2 carbons, and we plot all these data points in figure 5(b), as is usually done for inelastic neutron scattering determinations of the phonon branches. The symbols in figure 5(b) show experimental values for highly ordered pyrolytic graphite (HOPG) [26, 28], pyrolytic graphite (PG) [26], single wall carbon nanotubes (SWNTs) [17, 29, 30], ¹²C ion implanted HOPG (C-HOPG) [27], micro-crystalline graphite (MG) [18], and graphite whiskers (GW) [31].

This approach allows us to assign several Raman features previously observed for these materials. For example, Tan *et al* [31] reported two dispersive relatively lower phonon frequency modes in GW, which we assign to two of the three acoustic modes (iTAs and LA in figure 5(b)), which are resonant by an intra-valley scattering process. The frequency of the lowest optical branch at 849 cm⁻¹ (oTO) for $E_{laser} = 2.41$ eV should be difficult to observe in a Raman experiment. Here the letters ‘i’ and ‘o’ denote in-plane and out-of-plane phonon modes, respectively. The features around 1480 and 864 cm⁻¹ are assigned for the first time to

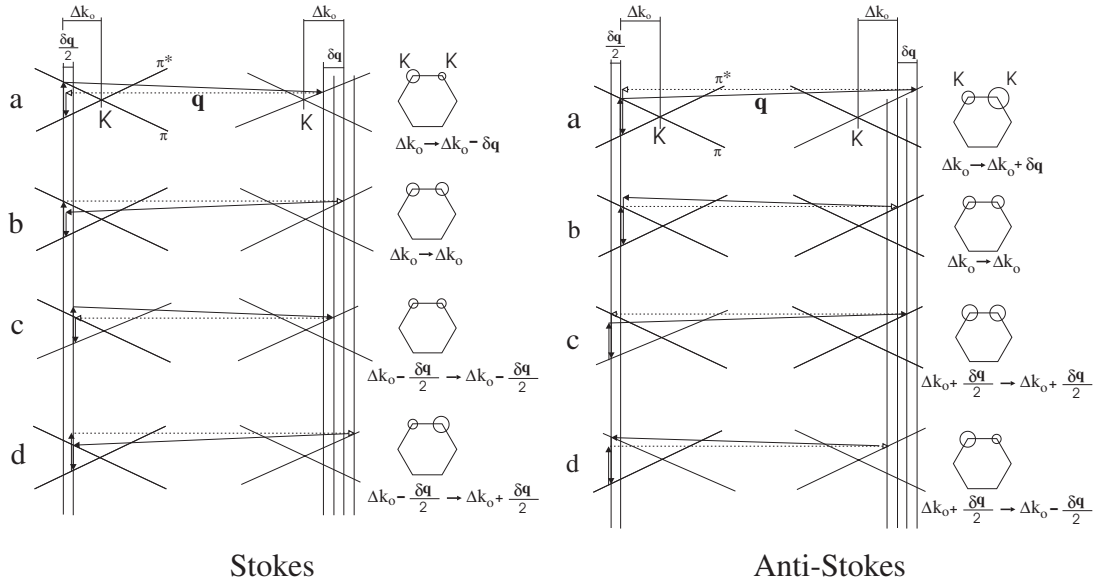


Figure 6. Four different second-order processes in the Stokes (left) and anti-Stokes (right) D-band Raman spectra (a and c) or (b and d) have the same lengths of q . Thus we expect to observe two peaks in the D-band spectra for disordered sp² carbon [25].

the iTO and oTO phonon branches, respectively. Furthermore, the broad weak signal around 1580 cm^{-1} which is a background of the strong G-band peaks, is assigned to the LO phonon branch ($q \sim 0$) near the Γ point [34, 35]. Around 1605 cm^{-1} , we can see weak features, denoted by D*, which originate from the top of the phonon dispersion relations of graphite. The D* band can be assigned to the intraband $q = 2k$ double resonance Raman spectra. It is noted here that some other groups use a different notation for D* and G'. The calculated frequencies and their dispersion are in excellent agreement with the experimental results for all of these features (see figure 5(b)). On the other hand, we can fit the phonon dispersion relation so as to reproduce the $q-E_{\text{laser}}$ pairs obtained from double resonance spectroscopy, whose results are shown in figure 5(c) [32]. The fitted phonon dispersion relations are different, especially around the K point, from that obtained using the original force constant set. This point should be clarified in detail in future experimental and theoretical work.

In solid state physics, the phonon dispersion relations of a solid are determined by either (1) neutron scattering measurements or (2) angle-resolved electron energy loss spectroscopy data. Thus double resonance Raman spectroscopy is an alternative method for obtaining the phonon dispersion relations for graphite-related materials [16, 24]. The merits of this method are: (a) no large single crystal is needed, (b) a disordered sample is preferable, (c) the accuracy of the method is similar throughout the BZ even at the zone-boundary.

Finally, to explain Feature 3, we should consider the length of q for the four different one-phonon, second-order processes for Stokes and anti-Stokes shifts, as shown in figure 6 [25]. The processes (b1)–(b4) in figure 1 correspond to a–d in figure 6 for intervalley scattering, which is relevant to the D and G' bands. For a given laser energy and phonon energies, the intermediate states around the K' point show four different $k + q$ states for each of the Stokes and anti-Stokes processes. For each case, the processes a and c have the same q vector, and

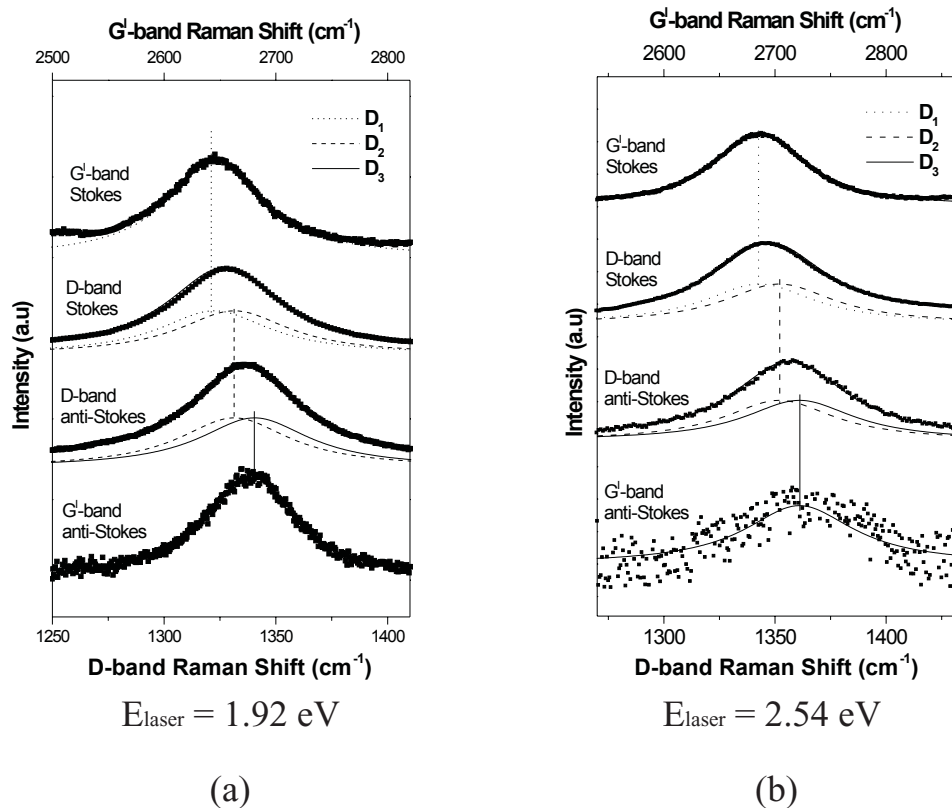


Figure 7. Stokes and anti-Stokes spectra of the D and G' bands for disordered graphite with (a) $E_{\text{laser}} = 1.92 \text{ eV}$ and (b) $E_{\text{laser}} = 2.54 \text{ eV}$. To compare with the D-band frequency (lower horizontal axis), the G'-band frequency is scaled by half (upper horizontal axis). Stokes and anti-Stokes shifts are shown [25].

the processes b and d also have the same q vector but different from a and c. Thus there are two different phonon frequencies for Stokes (or anti-Stokes) shifts of the D band. One of two D frequencies in the Stokes and anti-Stokes processes are the same, and is denoted by D_2 . The D_2 frequency corresponds to the process b, indicating that the resonance is with the incident photon and that the elastic scattering event occurs first. This gives the same q for Stokes and anti-Stokes processes. Let us denote the other frequencies in the Stokes and anti-Stokes spectra, respectively, by D_1 and D_3 ($D_1 < D_2 < D_3$).

In the case of two-phonon second-order Raman scattering, only the a and d processes in figure 6 are possible by changing the elastic process to an inelastic process. In this case q for process d becomes smaller (or larger) for the Stokes (or anti-Stokes) spectra and becomes the same q vector as for the process a. Thus the two processes a and d for the G' band merge into a single frequency which is exactly twice that of D_1 (or D_3) [25].

In figure 7, we plot the Stokes and anti-Stokes spectra of the D and G' bands for disordered graphite, with (a) $E_{\text{laser}} = 1.92 \text{ eV}$ and (b) $E_{\text{laser}} = 2.54 \text{ eV}$. We intentionally fit the D and G' bands by two and one Lorentzians (Lorentzian is a function for resonance phenomena [3, 4]), respectively, and the fitted results show that the above analysis fits the experimental data quite well [25]. Since this fitting procedure works at a different laser excitation energy, we can conclude that only double resonance theory can explain Feature 3.

4. D band of nanotube

In the case of SWNTs, the 2D electronic and phonon energy dispersion relations of graphite are zone-folded along the circumferential direction, which is realized by cutting the 2D BZ by lines, to obtain a set of 1D energy dispersion relations for SWNTs [14, 36]. The double resonance theory of graphite can be applied to SWNTs based on either the zone-folded BZ or on cutting lines in the extended 2D BZ. For simplicity, we explain the double resonance in the unfolded 2D BZ. Since optical absorption is necessary in the resonance Raman process, van Hove singularities in the JDOS are essential for obtaining a strong photo absorption (or emission) and for Raman spectra from a single nanotube. Each van Hove singularity in the JDOS comes from the flat energy dispersion point on the cutting line, denoted by k_i [6, 37]. When the initial (final) k and (or) the scattered $k + q$ are van Hove singular k_i points, the corresponding D- and G'-band features are enhanced significantly [7].

In the case of the G' band of SWNTs, it is not generally possible that both k and $k + q$ are simultaneously k_i points, since the $E(k)$ and $E(k + q)$ states have different phonon energies. Thus, even if the double resonance condition was satisfied for the 1D k and $k + q$ vectors, either $E(k)$ or $E(k + q)$ would not correspond to an energy where a van Hove singularity occurs. An anomalous special situation might occur when the energy difference between two different E_{ii} 's of an SWNT coincides with the phonon energy [7]. This situation is possible for special metallic nanotubes, for which the van Hove singular DOS is split into two peaks by the trigonal warping effect [37, 38] and the split happens to equal a phonon frequency. By utilizing the momentum conservation in the unfolded 2D BZ for the electron–phonon interaction process, we conclude that such an anomalous resonance situation can only happen for intravalley $q = 2k$ or intervalley $q = 0$ scattering processes, because the two split VHSs in metallic SWNTs appear on two different sides of the K point.

In the case of the D-band of SWNTs, it is possible that both the k and $k + q$ wavevectors are k_i points, since the initial k and final $k + q$ states can have the same energy if the scattering process is elastic. As discussed in the previous section, there are four possible, one-phonon, second-order, double resonance processes. In the case of SWNTs, when both the initial and final states of the elastic process are real electronic states (b and c in figure 6), we expect a significant Raman intensity at the van Hove singularity. Since these two processes give different phonon frequencies, the observed D-band spectra of the SWNT should therefore be fitted by two Lorentzians [5, 6], which appear at different resonant laser excitation energies.

In the experiment, we observe the D-band spectra for an isolated single wall carbon nanotube when an optical transition occurs between VHSs from the valence to the conduction bands [39]. Because of this effect, we can explain an oscillatory behaviour of the D- and G'-band phonon frequencies versus E_{laser} observed in SWNT bundles [17] by the double resonance process [7, 37, 39]. When an equi-energy contour touches the cutting lines of the 1D BZ, the touching point corresponds to k_i . The resonant nature of a given intermediate frequency mode spectrum has been observed by a tunable laser [40]. The double resonance process occurs from (or to) k_i points in the case of SWNTs, while all k points on the energy contour are possible for 2D graphite. Thus for SWNTs, the contributing phonon q vectors are limited, and they are not isotropic around the K point, which is the case of 2D graphite (see figure 4). Thus in the case of SWNTs, the double resonance process not only determines the *distance* of the q vector from the K point, but also specifies the *direction* of the q vector.

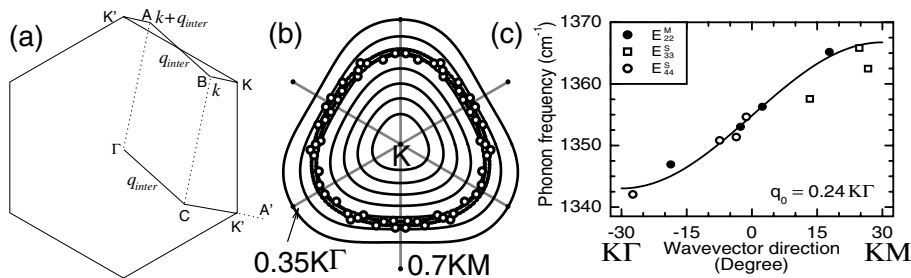


Figure 8. (a) Second-order scattering q vectors for a single wall carbon nanotube. A and B are the van Hove singular k_i points and the vector AB corresponds to the phonon wavevector. When we move the vector AB to Γ C, it is clear that $K'C = 2K'A'$ in which A' is equivalent to the A point in the 2D Brillouin zone [5]. (b) Phonon equi-frequency contours (solid lines), the experimental q -points (open circles), and the corresponding electronic equi-energy contours (dotted lines). (c) Dependence of ω_{ph} (\mathbf{q}) on the q -vector direction for a given q magnitude $q_0 = 0.24 \text{ K}\Gamma$. The frequency difference for two different q -vector directions KM and $K\Gamma$, $\Delta\omega_{\text{ph}} = 24 \text{ cm}^{-1}$ [6].

Since the direction of the cutting lines depends on the chiral angle [14], the chirality dependence of ω_D for isolated SWNTs is well explained by the distance of the k_i points from the K point [39]. The inter-valley phonon q vectors which connect two k_i points A and B are shown in figure 8(a). When A is located at k_i , the inequivalent B point is located at $-k_i$, and for any position of k_i , we can shift A and B to the nearest K' and K points as shown in figure 8(a), using the periodicity of k in the BZ. Further, when we shift the A point to the Γ point, the final point B moves to C which lies at $-2k_i$ position from the same K' point. Thus, the phonon frequency of the D band is relevant to the k_i distance, and more precisely to the opposite side of k_i from the K point. Since the trigonal warping effect affects both the k_i position and the phonon frequency, a chirality dependence of the D-band frequency was observed [39].

The chirality dependence of the double resonance Raman feature frequency arises from anisotropy (trigonal warping effect) of both the electronic dispersion relations [39] and the phonon dispersion relations [6] around the K point, because of the chirality dependence of the q vector direction, as discussed above. By measuring the double resonance Raman spectra from SWNTs of different chiralities for a given laser excitation energy, one can extract information regarding the phonon trigonal warping effect along the electronic equi-energy contours around the Γ and K points in the 2D BZ of the graphene layer. The phonon frequencies obtained from double resonance Raman features must be up-shifted to account for the force constant softening induced by the curvature of the SWNT wall [41]. Such measurements are very sensitive to the electronic trigonal warping effect, which determines the magnitudes of the k vector for different SWNT chiralities. The electronic trigonal warping effect, which is known from experimental studies of graphite and SWNTs as well as from theory [38], needs to be decoupled from experimental data of double resonance Raman frequencies for a proper determination of the phonon trigonal warping effect. Following this procedure, the trigonal warping effect of the iTO phonon mode around the K point has been measured from the G'-band frequencies of 11 individual SWNTs of different chiralities and similar diameters probed at the 514.5 and 488 nm Ar ion laser lines [6]. Figure 8(b) plots the

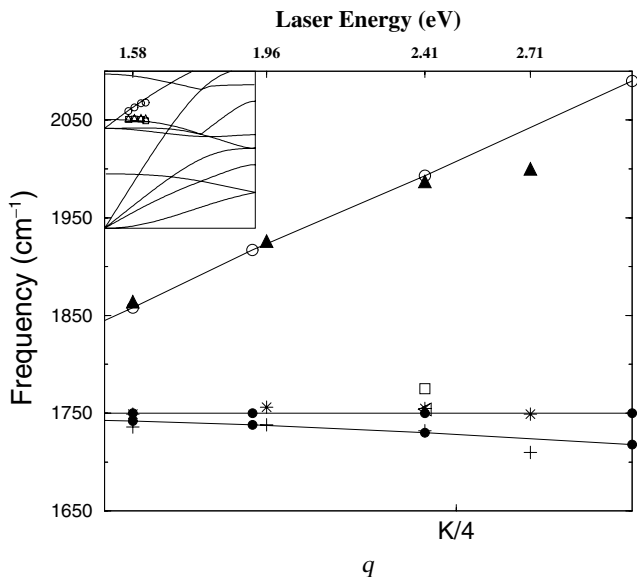


Figure 9. Frequency of the 2oTO (+) and iTO + LA (filled triangles) Raman features in SWNT bundles versus E_{laser} . The filled circles and open circles represent the frequencies of the calculated 2oTO and iTO + LA modes, respectively [8].

phonon equi-frequency contours, which clearly show the trigonal warping type effect, i.e., the contour anisotropy around the K point. Figure 8(c) shows the chirality dependence of the iTO phonon mode frequency for SWNTs with a mean diameter of 1.4 nm. The value of 24 cm⁻¹ for the variation of ω_{iTO} due to trigonal warping is not a negligible value [6], compared with the slope of the G'-band frequency.

5. Other intermediate phonon modes

Finally, we briefly mention some other peaks which are related to two-phonon modes. There are several overtone and combination phonon modes appearing in graphite-based materials. Using the double resonance theory, we assign specific combination modes to these features in the Raman spectra. An important fact for assigning the combination mode is that we cannot expect to observe a combination mode of intra-valley ($q \sim \Gamma$) and inter-valley ($q \sim K$) scattering, since the different q vectors cannot be selected in a second-order Raman process.

For two-phonon modes, it is not easy to do an assignment of the combination modes for conventional graphite, since the signal of two-phonon scattering becomes broader than that for one-phonon scattering. Thus an SWNT bundle is suitable for finding a signal if the resonance Raman condition is fulfilled.

In figure 9 we show the results for the Raman features that appear in an SWNT bundle. Two features appear in the resonance Raman spectra at around 1750 cm⁻¹ and we call these features the M band. The M-mode feature is interpreted as an overtone mode of the oTO phonon modes. The upper feature mode has a large dispersion around 1850–2050 cm⁻¹ and is identified with a combination mode of iTO and LA phonon modes, and therefore this mode is called iTOLA.

Table 1. Raman mode frequencies of carbon materials.

Name	ω [cm ⁻¹] ^a	Res. ^b	$\partial\omega/\partial E$ ^c	Notes ^d
iTA	288	DR1	129	TA mode, intraV ($q = 2k$)
LA	453	DR1	216	LA mode, intraV ($q = 2k$)
RBM	248/ d_t	SR	0	SWNT vibration of radius
oTO	860	DR1	0	oTO mode, intraV ($q = 0$)
oTO	865	DR1	13	oTO mode, intraV ($q = 2k$)
D	1350	DR1	53	LO mode, interV ($q = 2k$)
iTO	1450	DR1	0	LO mode, interV ($q = 0$)
BWF	1550	SR	0	Metallic SWNT, GIC
G	1590	SR	0 ^e	Raman active mode
D*	1605	DR1	~0	Top of phonon DOS
M	1750	DR2	26	Overtone of oTO mode
iTOLA	1950	DR2	230	TO + LA
G'	2700	DR2	106	Overtone of D mode
2iTO	2900	DR2	10	Overtone of LO mode ^f
2G	3180	DR2	0	Overtone of G mode

^aThe frequency is observed at $E_{\text{laser}} = 2.41$ eV.

^bSR: first-order Raman, DR1: one phonon double resonance Raman, DR2: two phonons, double resonance Raman.

^cThe change of phonon frequency (in cm⁻¹) by changing the laser energy by 1 eV.

^dintrav: intravalley scattering, interv: intervalley scattering. Most values of ω and the slope $\partial\omega/\partial E$ are taken from graphite-related materials. The values for SWNTs might be shifted. See text for the corresponding references.

^eThe value of $\partial\omega/\partial E$ is finite for a double resonance process (see text).

^fThis value is taken from the work of Tan *et al* [42].

Maultzsch and co-workers proposed that the G-band modes in graphite and SWNTs, which have been understood as first-order Raman active modes, are *entirely* double resonance Raman processes [24, 35]. The phonon energy dispersion for the highest phonon mode (LO) increases in energy with increasing k value from the point Γ (see figure 5) [14, 32] which can be seen by double resonance Raman spectroscopy as discussed in section 3 [16]. Group theory tells us, on the other hand, that the G band is the Raman-active mode of graphite [14]. The G-band feature is always strong, which does not depend on the number of defects. Thus the first-order Raman process should work except when there are any special reasons that suppress the first-order process. Thus further work is needed to understand the relationship between first-order and double resonance processes for the G band.

In table 1 we list all Raman spectra observed in graphite and SWNTs, where not only first-order Raman, but also the second-order Raman spectral features are included. Mainly, the slopes of the dispersive phonon modes for graphitic materials are also given.

6. Summary

In summary, using double resonance Raman theory, we can assign many known weak Raman features of carbon materials appearing below 3000 cm⁻¹. The dispersive nature of these Raman features and the discrepancy between phonon frequencies of the Stokes and anti-Stokes spectra can be explained. Further, the phonon dispersion relations can be obtained by analysing many peaks from many experiments. In the case of SWNTs, by including the singularities in the JDOS, we can get sharp double resonance Raman peaks, which are suitable even for obtaining the anisotropy of the phonon dispersion relations.

Such information provides not only a standard evaluation of SWNTs and graphite materials, but also contributes significantly to fundamental progress in resonance Raman spectroscopy. In the future, using a tunable laser and single nanotube spectroscopy, we should be able to get detailed information on the electronic and phonon structure of a single nanotube from experiments.

Acknowledgments

The authors acknowledge many experimental collaborators for providing important Raman spectra of SWNTs. RS acknowledges a grant-in-aid (No. 13440091) from the Ministry of Education, Japan. GeGS, VWB, GD and MSD acknowledge support under NSF grants DMR 01-16042 and INT 00-00408. AJ and MAP acknowledge support by the Instituto de Nanociências, Brazil. AGSF acknowledges financial support from CAPES-Brazil under a PRODOC-22001018 grant.

References

- [1] Dresselhaus M S, Dresselhaus G and Avouris Ph 2001 *Carbon Nanotubes: Synthesis, Structure, Properties and Applications* (*Springer Series in Topics in Applied Physics* vol 80) (Berlin: Springer)
- [2] Jorio A, Pimenta M A, Souza Filho A G, Saito R, Dresselhaus G and Dresselhaus M S 2003 *New J. Phys.* **5** 139
- [3] Cardona M 1982 *Light-Scattering in Solids*, ed M Cardona and G Güntherodt (Berlin: Springer) p 19
- [4] Martin R M and Falicov L M 1975 *Light-Scattering in Solids*, ed M Cardona (Berlin: Springer) p 80
- [5] Saito R, Jorio A, Souza Filho A G, Dresselhaus G, Dresselhaus M S, Grüneis A, Cançado L G and Pimenta M A 2002 *Japanese J. Appl. Phys. Part 1* **41** 4878
- [6] Samsonidze Ge G, Saito R, Jorio A, Souza Filho A G, Grüneis A, Pimenta M A, Dresselhaus G and Dresselhaus M S 2003 *Phys. Rev. Lett.* **90** 027403
- [7] Kürti J, Zólyomi V, Grüneis A and Kuzmany H 2002 *Phys. Rev. B* **65** 165433
- [8] Brar V W, Samsonidze Ge G, Dresselhaus G, Dresselhaus M S, Saito R, Swan A K, Ünlü M S, Goldberg B B, Souza Filho A G and Jorio A 2002 *Phys. Rev. B* **66** 155418
- [9] Souza Filho A G, Jorio A, Samsonidze Ge G, Dresselhaus G, Saito R and Dresselhaus M S 2003 *Nanotechnology* **14** 1130
- [10] Dresselhaus M S, Dresselhaus G, Jorio A, Souza Filho A G and Saito R 2002 *Carbon* **40** 2043
- [11] Tuinstra F and Koenig J L 1970 *J. Chem. Phys.* **53** 1126
- [12] Dresselhaus M S and Eklund P C 2000 *Adv. Phys.* **49** 705
- [13] Thomsen C and Reich S 2000 *Phys. Rev. Lett.* **85** 5214
- [14] Saito R, Dresselhaus G and Dresselhaus M S 1998 *Physical Properties of Carbon Nanotubes* (London: Imperial College Press)
- [15] Dresselhaus M S, Dresselhaus G and Eklund P C 1996 *Science of Fullerenes and Carbon Nanotubes* (New York: Academic)
- [16] Saito R, Jorio A, Souza Filho A G, Dresselhaus G, Dresselhaus M S and Pimenta M A 2002 *Phys. Rev. Lett.* **88** 027401
- [17] Pimenta M A, Hanlon E B, Marucci A, Corio P, Brown S D M, Empedocles S A, Bawendi M G, Dresselhaus G and Dresselhaus M S 2000 *Brazilian J. Phys.* **30** 423
- [18] Pócsik I, Hundhausen M, Koós M and Ley L 1998 *J. Non-Cryst. Solids* **227–230** 1083
- [19] Matthews M J, Pimenta M A, Dresselhaus G, Dresselhaus M S and Endo M 1999 *Phys. Rev. B* **59** R6585
- [20] Wang Y, Aolsmeyer D C and McCreery R L 1990 *Chem. Mater.* **2** 557

- [21] Dresselhaus M S and Kalish R 1992 *Ion Implantation in Diamond, Graphite and Related Materials (Springer Series in Materials Science vol 22)* (Berlin: Springer)
- [22] Ferrari A C and Robertson J 2001 *Phys. Rev. B* **64** 075414
- [23] Ferrari A C and Robertson J 2000 *Phys. Rev. B* **61** 14095
- [24] Maultzsch J, Reich S, Schlecht U and Thomsen C 2003 *Phys. Rev. Lett.* **91** 087402
- [25] Cançado L G, Pimenta M A, Saito R, Jorio A, Ladeira L O, Grüneis A, Souza Filho A G, Dresselhaus G and Dresselhaus M S 2002 *Phys. Rev. B* **66** 035415
- [26] Kawashima Y and Katagiri G 1995 *Phys. Rev. B* **52** 10053
- [27] Tan P H, Deng Y M and Zhao Q 1998 *Phys. Rev. B* **58** 5435
- [28] Kawashima Y and Katagiri G 1999 *Phys. Rev. B* **59** 62
- [29] Alvarez L, Righi A, Rols S, Anglaret E and Sauvajol J L 2000 *Chem. Phys. Lett.* **320** 441
- [30] Tan P H, Tang Y, Deng Y M, Li F, Wei Y L and Cheng H M 1999 *Appl. Phys. Lett.* **5** 1524
- [31] Tan P H, Hu C Y, Dong J, Shen W C and Zhang B F 2001 *Phys. Rev. B* **64** 214301
- [32] Grüneis A, Saito R, Kimura T, Cançado L G, Pimenta M A, Jorio A, Souza Filho A G, Dresselhaus G and Dresselhaus M S 2002 *Phys. Rev. B* **65** 155405
- [33] Saito R, Takeya T, Kimura T, Dresselhaus G and Dresselhaus M S 1998 *Phys. Rev. B* **7** 4145
- [34] Jorio A, Pimenta M A, Souza Filho A G, Fantini C, Samsonidze Ge G, Dresselhaus G, Dresselhaus M S and Saito R 2003 *Proc. XVI Int. Winter School on Electronic Properties of Novel Materials* (Kirchberg Winter School, Austria), ed H Kuzmany, J Fink, M Mehring and S Roth (Woodbury, NY: American Institute of Physics)
- [35] Maultzsch J, Reich S and Thomsen C 2002 *Phys. Rev. B* **65** 233402
- [36] Samsonidze Ge G, Saito R, Jorio A, Pimenta M A, Souza Filho A G, Grüneis A, Dresselhaus G and Dresselhaus M S 2003 *J. Nanosci. Nanotechnol.* (in press)
- [37] Souza Filho A G *et al* 2002 *Chem. Phys. Lett.* **354** 62
- [38] Saito R, Dresselhaus G and Dresselhaus M S 2000 *Phys. Rev. B* **61** 2981
- [39] Souza Filho A G *et al* 2002 *Phys. Rev. B* **65** 035404
- [40] Fantini C *et al* unpublished
- [41] Souza Filho A G, Jorio A, Samsonidze Ge G, Dresselhaus G, Pimenta M A, Dresselhaus M S, Swan A K, Ünlü M S, Goldberg B B and Saito R 2003 *Phys. Rev. B* **67** 035427
- [42] Tan P H, An L, Liu L Q, Guo Z X, Czerw R, Carroll D L, Ajayan P M, Zhang N and Guo H L 2002 *Phys. Rev. B* **66** 245410